Attosecond imaging of photoinduced dynamics in molecules using time-resolved photoelectron momentum microscopy

Marvin Reuner[1] and Daria Popova-Gorelova [1,2]
[1]*I. Institute for Theoretical Physics and Centre for Free-Electron Laser Science,*
Universität Hamburg, Notkestraße 9, 22607 Hamburg, Germany
[2]*The Hamburg Centre for Ultrafast Imaging, Luruper Chaussee 149, 22607 Hamburg, Germany*

We explore the capabilities offered by attosecond extreme ultraviolet and x-ray pulses that can now be generated by free-electron lasers and high-order harmonic generation sources for probing photon-induced electron dynamics in molecules. We theoretically analyze how spatial and temporal dependence of charge migration in a pentacene molecule can be followed by means of time-resolved photoelectron microscopy on the attosecond timescale. Performing the analysis, we accurately take into account that an attosecond probe pulse leads to considerable spectral broadening. We demonstrate that the excited-state dynamics of a neutral pentacene molecule in real space map onto unique features of photoelectron momentum maps.

I. INTRODUCTION

Photoelectron momentum microscopy is a technique in which a light pulse ionizes a probe, leading to the detachment of a photoelectron. The momentum distribution of the detached photoelectron encodes information about the shape of an orbital or a bond in the real space from which the electron was detached [1–12]. This connection is facilitated by the Fourier transform, which links real and momentum space. The spatial resolution of this technique is given by the de Broglie wavelength of the emitted photoelectron, which is determined by the kinetic energy of the photoelectron. If an extreme ultraviolet (XUV) probe pulse detaches an electron from a valence orbital, the photoelectron would also have a kinetic energy in the XUV range corresponding to the resolution of a few angstroms.

In recent years, there has been remarkable progress in atomic-scale imaging of photoexcited states and dynamics using photoelectron momentum microscopy. Momentum-space distribution of transiently excited electrons was measured [13], the dynamics of crystalline bonds was followed during the photoinduced phase transition [9], and the technique allowed the detection of singlet fission with orbital resolution [14]. Time-resolved photoelectron momentum microscopy probing photoinduced dynamics of pentacene films on a sub-picosecond timescale has been achieved at the free-electron laser FLASH [15]. So far, these experiments have been performed at a subpicosecond timescale and have not been capable of capturing pure electron dynamics in real time on its natural timescale. This barrier is now possible to overcome due to the capabilities to produce attosecond x-ray pulses at free-electron lasers [16–18] or attosecond XUV pulses using high-order harmonic generation sources [19–25]. These sources were already successfully employed to study electronic processes with few-femtosecond to attosecond time

and atomic-scale space resolution [26–36], and different experimental schemes are being explored theoretically [37–49]. The interpretation of a signal from attosecond probe pulses is challenging since they have a broad bandwidth in the energy domain, which smears out spectral lines in a signal. In this article, we analyze how attosecond XUV pulses can be employed to measure charge migration in a pentacene molecule and analyze how to extract the real-space and real-time information about charge migration using momentum-resolved photoelectron microscopy.

Pentacene is a prototypical organic semiconductor composed of pentacene molecules which is among candidate materials for efficient organic photovoltaics [50,51]. The understanding of the process of solar-energy conversion in organic semiconductors strongly relies on the insight into both intra- and intermolecular photoexcited processes [52]. Exciton migration is one of the fundamental processes governing solar-energy conversion, and the role of electronic coherence processes becomes especially relevant near conical intersections [53–55]. Electronic charge-migration dynamics launched as a coherent superposition of electronic states has already been studied in detail [56–65]. In this article, we focus on the description of how such coherent electron dynamics can be probed on the nanoscale by broadband probe pulses. Particularly, we study how attosecond photoelectron momentum microscopy can be employed to probe intramolecular coherent exciton dynamics in pentacene.

It has been shown that time-resolved photoelectron spectroscopy can be applied to probe ultrafast electronic and nuclear molecular dynamics [43,66–71]. However, angle-unresolved photoelectron spectra do not carry any spatial information about the dynamics, which is lost due to angle averaging. In photoelectron momentum microscopy, the momentum distribution of photoelectrons is detected. The great advantage of this technique over angle-averaged spectroscopy

is that the distribution provides details of electron dynamics within a molecule if photoelectrons are detached with high kinetic energies. We will also show that photoelectron spectra can lose important time-resolved information about the dynamics after angle averaging.

In this article, we apply the general theoretical formalism to describe the time- and momentum-dependent photoelectron probability by a broad-bandwidth probe pulse derived in Ref. [7]. That study proposed probing hole dynamics in a positively ionized molecule by emitting electrons from orbitals that were initially occupied. Here, we propose applying attosecond XUV pulses to probe photoexcited states of a neutral molecule, which is especially relevant for revealing information about exciton dynamics in the energy conversion processes.

This article is organized as follows. We develop the theoretical description of time-resolved photoelectron momentum microscopy of excited-state dynamics in molecules while taking electron correlations and the broad bandwidth of a probe pulse into account in Sec. II. In Sec. III, we calculate photoelectron spectra and photoelectron momentum maps from coherent electron-hole dynamics in a pentacene molecule obtained by an attosecond XUV probe pulse. We reveal how time-resolved atomic-scale changes in electron density are correlated with time-resolved changes in photoelectron momentum maps.

II. METHOD

Throughout this article, we consider a molecule with coherently evolving electron dynamics. In this case, the N_{el}-electron wave function of a molecule is a coherent superposition of several excited electronic eigenstates $|\Phi_I\rangle$,

$$|\Psi(t)\rangle = \sum_I C_I e^{-iE_I(t-t_0)}|\Phi_I\rangle, \qquad (1)$$

where E_I is the corresponding eigenenergy and the coefficient C_I determines the population distribution for each eigenstate. The coherent superposition emerges at time t_0 due to the crossing of a conical intersection or excitation by a pump pulse. We assume that an ultrashort XUV probe pulse interacts with the molecule at time t_p, which leads to an emission of a photoelectron. The momentum distribution of the photoelectron encodes information about the electronic state at time t_p. In our study, we propose to probe electron dynamics by studying the momentum distribution of photoelectrons emitted from the outermost orbitals that became populated due to the photoexcitation of the molecule. We use atomic units for this and the following expressions.

Assuming a probe pulse with the central photon energy ω_{in}, polarization ϵ_{in}, pulse duration τ_p, and intensity profile $I(t) = I_0 e^{-4\ln 2[(t-t_p)/\tau_p]^2}$, the general expression for the photoelectron probability is [7]

$$P(\mathbf{q}, t_p) = \frac{\tau_p^2 I_0 |\epsilon_{in} \cdot \mathbf{q}|^2}{8\pi \ln 2 \omega_{in}^2 c} \sum_{F,\sigma} e^{-(\Omega_F - \epsilon_e)^2 \tau_p^2/(4\ln 2)}$$

$$\times \left| \chi_\sigma^\dagger \int d^3r \, e^{-i\mathbf{q}\cdot\mathbf{r}} \phi_F^D(\mathbf{r}, t_p) \right|^2, \qquad (2)$$

where $\mathbf{q}$ is the momentum of the photoelectron with the corresponding energy $\epsilon_e = \frac{|\mathbf{q}|^2}{2}$ and χ_σ is the photoelectron spin state. The summation is over all possible final states of the molecule $\langle\Phi_F^{N_{el}-1}|$ that can be produced after the photoionization by the probe pulse, and E_F is their corresponding eigenenergy. $\phi_F^D(\mathbf{r}, t_p) = \langle\Phi_F^{N_{el}-1}|\hat{\psi}(\mathbf{r})|\Psi(t_p)\rangle$ is the Dyson orbital defined as the overlap between the N_{el} wave function of the initial state of the system and the $(N_{el} - 1)$ wave function of the final state, where $\hat{\psi}(\mathbf{r})$ is the electron annihilation field operator. $\Omega_F = \omega_{in} + \langle E\rangle - E_F$, where $\langle E\rangle$ is the mean energy of the eigenstates involved in the wave packet in Eq. (1). Here, we assume the sudden approximation, i.e., the molecular state after photoionization and the state of the photoelectron are decoupled, which is justified for high kinetic photoelectron energies [72]. It is also assumed that the probe-pulse duration is much shorter than the characteristic timescale of the electron dynamics. This means that the energy splittings of the eigenstates involved in the dynamics are much smaller than the bandwidth of the probe pulse and can be substituted by their mean energy. If this assumption fails, the eigenenergies must enter the expression explicitly, and Eq. (2) gets slightly modified:

$$P(\mathbf{q}, t_p) \propto \sum_{F,\sigma} \left| \sum_I e^{-(\omega_{in} + E_I - E_F - \epsilon_e)^2 \tau_p^2/(8\ln 2)} \right.$$

$$\left. \times \chi_\sigma^\dagger \int d^3r \, e^{-i\mathbf{q}\cdot\mathbf{r}} \phi_{FI}^D(\mathbf{r}, t_p) \right|^2, \qquad (3)$$

where $\phi_{FI}^D(\mathbf{r}, t_p) = \langle\Phi_F^{N_{el}-1}|\hat{\psi}(\mathbf{r})|C_I e^{-iE_I(t_p-t_0)}\rangle$. The time- and angle-resolved photoelectron probability for molecules with electron dynamics was also previously studied theoretically [66,73–75]. Equations (2) and (3) take the broad bandwidth of a probe pulse accurately into account, which was not the case in those studies.

It follows from expression (2) that the momentum-resolved photoelectron probability encodes the Fourier transform of the Dyson orbital. If the molecule is in the ground state, the overlap integral between a singly ionized molecule and the molecule before the ionization is well approximated by the Hartree-Fock (HF) orbital, from which an electron was detached. Due to this connection, photoelectron momentum microscopy is used as an orbital imaging method [2,76,77].

When a molecule in an excited state is ionized by a probe pulse, the Dyson orbital cannot be approximated by a molecular orbital, and the interpretation of the Dyson orbital becomes more challenging. In order to carefully describe the excited-state dynamics as well as to accurately treat the Dyson orbital, we describe the excited states involved in the dynamics Φ_I and the states of the ionized molecule $\Phi_F^{N_{el}-1}$ using the configuration-interaction method. We express each excited state based on the configuration-interaction approach limited to single excitations as

$$|\Phi_I\rangle = \sum_{i_1, a_1} \tilde{c}_{i_1}^{a_1}(I) |\phi_{i_1}^{a_1, S(I)}\rangle, \qquad (4)$$

where $|\phi_{i_1}^{a_1,S(I)}\rangle$ denotes a configuration-state function (CSF), where an electron of the HF ground state has been excited from orbital i_1 to orbital a_1. Such a state has a hole in orbital i_1 and an electron in orbital a_1, and $S(I)$ describes the total spin and the spin-projection value. For the description of the final state, we use a similar approach but add one additional hole in the configuration space. Thus, the final state is

$$\langle\Phi_F^{N_{el}-1}| = \sum_{i_2,j_2,a_2}\tilde{c}_{i_2,j_2}^{a_2}(F)\langle\phi_{i_2,j_2}^{a_2,S(F)}| + \sum_{i_2}\tilde{c}_{i_2}(F)\langle\phi_{i_2}^{S(F)}|, \quad (5)$$

where $\langle\phi_{i_2,j_2}^{a_2,S(F)}|$ describes a CSF which contains two holes in orbitals i_2 and j_2 and an electron in orbital a_2. We denote an $(N_{el}-1)$-electron CSF with one hole among originally occupied orbitals of the molecule [highest occupied molecular orbital (HOMO), HOMO − 1, . . .] and no electrons in the originally unoccupied molecular orbitals [lowest unoccupied molecular orbital (LUMO), LUMO + 1, . . .] as $\langle\phi_{i_2}^{S(F)}|$. In both cases, $S(F)$ describes the total spin and the spin-projection value of the final state F. The coefficients $\tilde{c}_{i_2,j_2}^{a_2}(F)$ and $\tilde{c}_{i_2}(F)$ determine the contribution of a CSF to the final state. We perform calculations employing the RASSCF method [78] and use the same active orbitals for the treatment of states $|\Phi_I\rangle$ and $\langle\Phi_F^{N_{el}-1}|$. With these approximations, the overlap integrals between neutral and singly ionized eigenstates of a molecule are given by a linear combination of the overlap integrals between N_{el}- and $(N_{el}-1)$-electron CSFs. Such an overlap integral provides either a zero or a molecule orbital, which is occupied in an N_{el}-electron CSF and unoccupied in an $(N_{el}-1)$-electron CSF. Thus, a Dyson orbital can be represented as a linear combination of molecular orbitals.

III. IMAGING PHOTOINDUCED DYNAMICS IN PENTACENE

Based on the previous considerations, we present an example for imaging excited-state dynamics in aligned isolated pentacene molecules. The molecular alignment can be achieved either for gas-phase molecules or for molecular films adsorbed on substrates. We recently observed that the photoexcited dynamics of pentacene molecules in the top pentacene layer of a bilayer pentacene film adsorbed on an Ag(110) surface behaves similarly to the dynamics of isolated pentacene [15]. These dynamics were probed using time-resolved photoelectron momentum microscopy on a timescale of several hundreds of femtoseconds. This experiment established conditions for time-resolved photoelectron microscopy at free-electron lasers, which makes it feasible to perform such experiments at much shorter timescales with brilliant and ultrashort light pulses from free-electron laser sources.

In our study, we assume that coherent electron dynamics in pentacene were excited by a pump pulse via an optical excitation from the ground state. Since direct optical transitions from the ground state to triplet excited states are dipole forbidden, we truncate our considerations to spin-singlet excited states.

We calculate the vertical excited spin-singlet states of pentacene with MOLCAS [79] using the RASSCF method [78], with a correlation-consistent polarized valence double zeta
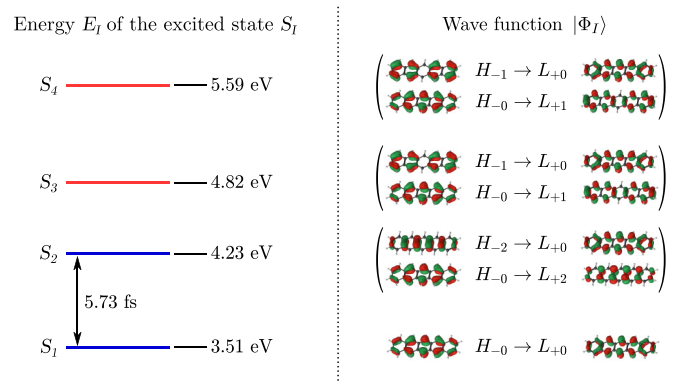

FIG. 1. Energy-level diagram of the first four vertical spin-singlet excited states of pentacene (left), with bright states S_1 and S_2 in blue and dark states S_3 and S_4 in red. A wave packet in a coherent superposition of the first two excited states has an oscillation period of 5.73 fs. The corresponding orbital excitations contribute to the wave function of the states (right), while the arrow means an excitation from the left (HOMO − i) to the right (LUMO + j) orbital. For the visualization of the orbitals, we used the software LUSCUS [82]

(cc-pVDZ) basis set for the atoms [80,81]. The calculation of the first excited states of pentacene is converged with an active space of 22 orbitals, containing 11π and $11\pi^*$ orbitals. Including more orbitals in the active space does not lead to significant changes in the energy spectrum and the structure of the eigenstates. The π orbitals contain a maximum of one hole, while the π^* orbitals have a maximum of one electron. The energies of the first four excited states and the changes in the occupation of the orbitals (compared to the HF ground state) are shown in Fig. 1. We find that the third and fourth excited singlet states are dark states and the next bright singlet states are energetically highly separated from the first and second excited states. Thus, one would be able to create a coherent superposition of just two excited states of pentacene in a possible experiment. When the coherent superposition of the two excited states of pentacene is created, its electron density starts to oscillate in time. The oscillation period is determined by the energy difference between the excited states. The energy difference and the electronic wave functions of the bright excited states obtained in our calculation agree well with the experimental and theoretical results in previous studies [83–85]. Also, the agreement with a more accurate CASPT2 calculation [85] justifies our chosen theoretical level of single excitation in the configuration space. We find that the first excited state is predominantly characterized by the CSF obtained by the excitation of an electron from the HOMO to the LUMO. The second excited state is predominantly characterized by a linear combination of the CSF obtained by the excitation of an electron from the HOMO to the LUMO + 2 and the CSF obtained by the excitation of an electron from the HOMO − 2 to the LUMO.

The energy difference between the two excited states results in an oscillation period of the electron density of $T = 5.73$ fs. To simplify our considerations, we can neglect nuclear motions that should affect electron dynamics on longer timescales. With Eq. (1) the time evolution of the wave packet

after the excitation by the pump pulse at $t_0 = 0$ is

$$|\Psi(t)\rangle = C_1 e^{-iE_1 t}|\Phi_1\rangle + C_2 e^{-iE_2 t}|\Phi_2\rangle, \qquad (6)$$

$$|\Phi_1\rangle = |\phi_H^{L,0(0)}\rangle, \qquad (7)$$

$$|\Phi_2\rangle = \frac{1}{\sqrt{2}}\left(|\phi_H^{L+2,0(0)}\rangle - |\phi_{H-2}^{L,0(0)}\rangle\right), \qquad (8)$$

with $|C_1|^2 + |C_2|^2 = 1$. The coefficients C_1 and C_2 depend on a particular process which brings a molecule into a coherent superposition of electronic states. Our results do not depend on the particular values of coefficients C_1 and C_2, and we assume an equal population of both excited states, $C_1 = C_2 = \frac{1}{\sqrt{2}}$. The orbital index $H - i$ denotes the ith orbital below the HOMO, and $L + j$ is the jth orbital above the LUMO. The photoexcitation leads to a time-dependent change in the electron density relative to the ground-state density,

$$\rho_{ex}(\mathbf{r}, t) = \rho_1(\mathbf{r}, t) - \rho_0(\mathbf{r}), \qquad (9)$$

where $\rho_0(\mathbf{r}) = \langle\Phi_0|\hat{\psi}^\dagger(\mathbf{r})\hat{\psi}(\mathbf{r})|\Phi_0\rangle$ is the electron density of the ground state of pentacene described by the wave function $|\Phi_0\rangle$. The electron density for pentacene after the photoexcitation by a pump pulse is $\rho_1(\mathbf{r}, t) = \langle\Psi(t)|\hat{\psi}^\dagger(\mathbf{r})\hat{\psi}(\mathbf{r})|\Psi(t)\rangle$. We evaluate the electron density change and obtain

$$\rho_{ex}(\mathbf{r}, t) = \left| C_1^* e^{iE_1 t}\phi_L(\mathbf{r}) + \frac{C_2^*}{\sqrt{2}}e^{iE_2 t}\phi_{L+2}(\mathbf{r}) \right|^2$$
$$+ \frac{|C_2|^2}{2}|\phi_L(\mathbf{r})|^2 - \frac{|C_2|^2}{2}|\phi_H(\mathbf{r})|^2$$
$$- \left| C_1^* e^{iE_1 t}\phi_H(\mathbf{r}) - \frac{C_2^*}{\sqrt{2}}e^{iE_2 t}\phi_{H-2}(\mathbf{r}) \right|^2, \qquad (10)$$

where $\phi_{H-i}(\mathbf{r})$ and $\phi_{L+j}(\mathbf{r})$ are the wave functions of the ith orbital below the HOMO and the jth orbital above the LUMO. The electron density change is shown in Fig. 2 at different times during the oscillation period. The negative (blue) part is the reduction of the electron density compared to the ground-state density, and the positive (yellow) part is the increase of the electron density compared to the ground-state density. The time-dependent part of the electron density oscillates in time as $\cos[(E_1 - E_2)t]$. From $t = 0$ to $t = \frac{T}{2}$, the photoinduced negative charge flows from the top left and bottom right of the molecule to the top right and bottom left. The photoinduced positive charge flows in the opposite direction. The spatial
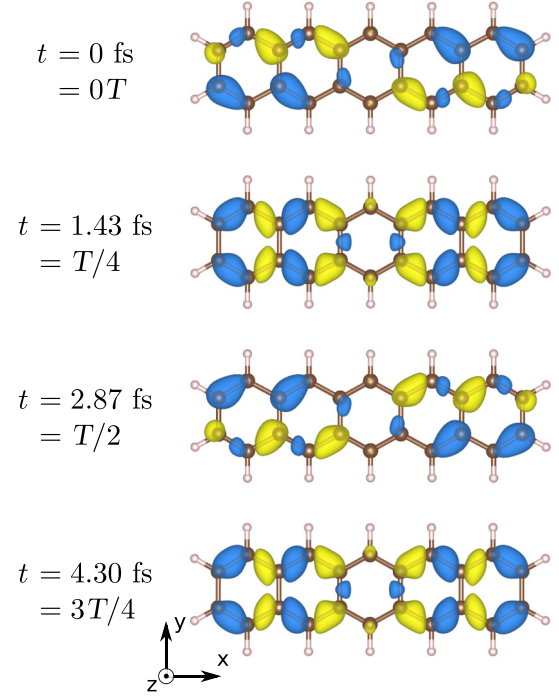

FIG. 2. The time evolution of the electron-hole density after the excitation of the pentacene molecule to the first two excited states with the pump pulse at $t_0 = 0$ fs. The blue isosurface shows the hole density (negative value), and the yellow one shows the electron density (positive value). For the visualization we used the software VESTA [86].

distribution of the electron density change at $t = \frac{T}{2}$ can be mapped onto the electron density change at $t = 0$ by a reflection in the yz plane. At two times during the oscillation period, $t = \frac{T}{4}$ and $t = \frac{3T}{4}$, the photoexcited change in the electron density coincides and has reflection symmetry. We assume that an XUV probe pulse with a central energy of 100 eV and 500-as duration photoionizes the molecule at the pump-probe time delay t_p. The probe pulse is linearly polarized along the y direction, which is perpendicular to the nodal plane of the molecule. For the calculation of the final states after the photoionization by the probe pulse, we apply the same method as in the calculation of the excited states of pentacene, but with an additional hole in the 11 active π orbitals. Table I shows

TABLE I. First six final states $\langle\Phi_F|$ of ionized and excited pentacene, which result in a nonzero Dyson orbital $\phi_F^D(\mathbf{r}) = \langle\Phi_F^{N_{el}-1}|\hat{\psi}(\mathbf{r})|\Psi(t)\rangle$. The corresponding energy is E_F, and $\Omega_F = E_F - \langle E\rangle - \omega_{in} + \epsilon_e$ is the central energy in the photoelectron probability in Eq. (2) for the given final state. The right column shows the contributing configuration-state functions of the final state. The indices udu and uud distinguish two different CSFs that result in a total spin of $1/2$ and spin projection of $+1/2$.

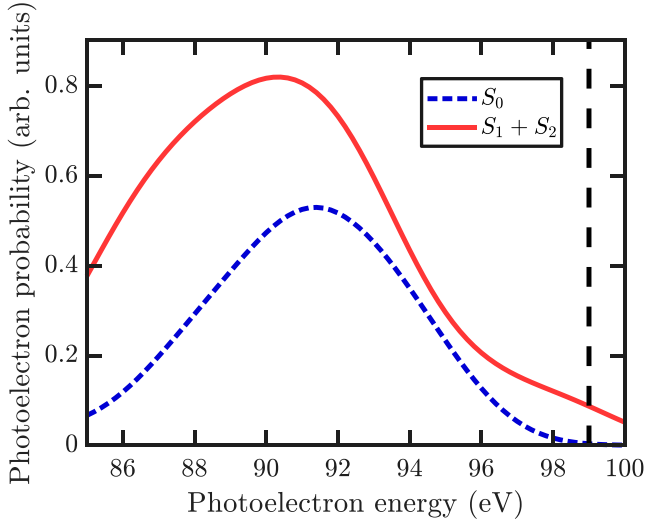| F	E_F (eV)	Ω_F (eV)	$\langle\Phi_F^{N_{el}-1}|$
1	5.0	98.9	$-0.95\langle\Phi_H^{1/2(1/2)}|$
2	6.7	97.2	$-0.94\langle\Phi_{H-2}^{1/2(1/2)}|$
3	7.5	96.4	$-0.83\langle\Phi_{H,H}^{L,1/2(1/2)}| + 0.31\langle\Phi_{H-4}^{1/2(1/2)}|$
4	8.7	95.2	$-0.62\langle\Phi_{H,H}^{L+1,1/2(1/2)}| + 0.5\langle\Phi_{H-1,H}^{L,1/2(1/2)}|_{udu} + 0.28\langle\Phi_{H-1,H}^{L,1/2(1/2)}|_{uud}$
5	9.6	94.3	$0.70\langle\Phi_{H-1,H}^{L,1/2(1/2)}|_{uud} - 0.45\langle\Phi_{H-1,H}^{L,1/2(1/2)}|_{udu}$
6	9.7	94.2	$-0.59\langle\Phi_{H,H}^{L+2,1/2(1/2)}| + 0.62\langle\Phi_{H-2,H}^{L,1/2(1/2)}|_{udu} - 0.28\langle\Phi_{H-2,H}^{L,1/2(1/2)}|_{uud}$

FIG. 3. Angle-integrated photoelectron spectra for photoelectrons either detached from the ground state S_0 or in the coherent superposition of the excited states S_1 and S_2. The vertical black dashed line shows the contribution at the photoelectron energy $\epsilon_e = 99$ eV. The probe-pulse duration is 0.5 fs and has a central photon energy of 100 eV.

the first six final states of pentacene with the lowest energy that can be reached by ionizing the initial state in Eq. (6).

If the photoionization was triggered by a pulse with a narrow bandwidth, the photoelectron probability as a function of energy would consist of clear spectral lines centered at energies $\Omega_{F,I} = E_F - E_I - \omega_{in} + \epsilon_e$. Thus, the photoelectron momentum distributions would be clearly assigned to a certain Dyson orbital. In the case of the ultrashort probe pulse, each spectral line has a spectral band width of 5.16 eV, and an individual Dyson orbital contributing to the momentum distribution at a given energy is no longer distinguished.

Let us first consider the angle-integrated photoelectron spectra. In a real experiment, a probe pulse would interact with a number of pentacene molecules, some of which would be excited by a pump pulse and some of which would remain unexcited. Thus, we first estimate how the photoionization from unexcited pentacene molecules would affect the photoelectron spectra from pentacene molecules in the excited state. In Fig. 3, we show photoelectron spectra from the pentacene molecules in the ground state S_0 and from pentacene molecules in the coherent superposition of the excited states S_1 and S_2 [$|\Psi(t)\rangle$ in Eq. (6)]. We find that the contribution of photoelectrons detached from unexcited molecules is negligible at energies higher than 97 eV. Thus, photoelectron spectra at energies higher than 97 eV are beneficial to study the dynamics of photoexcited pentacene molecules since they

would not contain a background signal from the unexcited molecules.

We find the remarkable result that the angle-averaged photoelectron spectra from photoexcited pentacene do not vary with the probe-pulse arrival time, although the photoinduced charge distribution experiences considerable oscillations in time (see Fig. 2). This is because the time-dependent part of the electronic density change is highly symmetric in space. As a consequence, the photoelectron momentum distributions are also highly symmetric, and the temporal dependence of the signal averages out after the angle integration. The angle-integrated spectra do not reveal information about the time-dependent photoinduced charge oscillations.

We now demonstrate that photoelectron momentum microscopy is, indeed, quite sensitive to photoinduced electron dynamics. We consider photoelectron momentum maps (PMMs) of a photoelectron with a fixed kinetic energy of $\epsilon_e = 99$ eV. PMMs are constructed by a two-dimensional projection of the three-dimensional photoelectron momentum distribution for a constant energy ϵ_e (hemispherical cuts). Based on Eq. (2), the photoelectron probability resulting from a particular final state is only time dependent if the final state has a nonzero overlap with both eigenstates in the initial state, $\langle \Phi_F | \hat{\psi}(\mathbf{r}) | \Phi_1 \rangle \neq 0$ and $\langle \Phi_F | \hat{\psi}(\mathbf{r}) | \Phi_2 \rangle \neq 0$. At the chosen kinetic energy, three final states with the lowest energies, with the indices 1, 2, and 3 in Table I, contribute to the PMM. Among these three final states, only final state 1 contributes to a time-dependent signal, and the other two final states, 2 and 3, contribute to a time-independent background. The first final state results in a broad spectral line centered approximately at energy $\epsilon_e = 99$ eV.

We derive the explicit expressions for the Dyson orbital that determine the angle-resolved photoelectron spectra at $\epsilon_e = 99$ eV. For the first three final states, we obtain

$$
\begin{aligned}
\phi_{F_1}^D(\mathbf{r}) &= \langle \Phi_{F_1} | \hat{\psi}(\mathbf{r}) | \Psi(t) \rangle \\
&= -C_1 e^{-iE_1 t_p} \frac{0.95}{\sqrt{2}} \phi_L(\mathbf{r}) \chi_\downarrow \\
&\quad - C_2 e^{-iE_2 t_p} \frac{0.95}{2} \phi_{L+2}(\mathbf{r}) \chi_\downarrow,
\end{aligned} \tag{11}
$$

$$
\begin{aligned}
\phi_{F_2}^D(\mathbf{r}) &= \langle \Phi_{F_2} | \hat{\psi}(\mathbf{r}) | \Psi(t) \rangle \\
&= C_2 e^{-iE_2 t_p} \frac{0.94}{2} \phi_L(\mathbf{r}) \chi_\downarrow,
\end{aligned} \tag{12}
$$

$$
\begin{aligned}
\phi_{F_3}^D(\mathbf{r}) &= \langle \Phi_{F_3} | \hat{\psi}(\mathbf{r}) | \Psi(t) \rangle \\
&= -C_1 e^{-iE_1 t_p} \frac{0.83}{\sqrt{2}} \phi_H(\mathbf{r}) \chi_\downarrow.
\end{aligned} \tag{13}
$$

The three Dyson orbitals in Eqs. (11)–(13) enter the photoelectron probability in Eq. (2) at photoelectron energy $\epsilon = 99$ eV,

$$
\begin{aligned}
P(\mathbf{q}, t_p) \underset{\epsilon_e = 99 \text{ eV}}{\propto} |\boldsymbol{\epsilon}_{in} \cdot \mathbf{q}|^2 &\left[e^{-(\Omega_{F_1} - \epsilon_e)^2 \frac{\tau_p^2}{4 \ln 2}} \left| C_1 e^{-iE_1 t_p} \frac{0.95}{\sqrt{2}} \mathcal{F}(\phi_L(\mathbf{r}))(\mathbf{q}) + C_2 e^{-iE_2 t_p} \frac{0.95}{2} \mathcal{F}(\phi_{L+2}(\mathbf{r}))(\mathbf{q}) \right|^2 \right] \\
+ |\boldsymbol{\epsilon}_{in} \cdot \mathbf{q}|^2 &\left[e^{-(\Omega_{F_2} - \epsilon_e)^2 \frac{\tau_p^2}{4 \ln 2}} \left| C_2 \frac{0.94}{2} \mathcal{F}(\phi_L(\mathbf{r}))(\mathbf{q}) \right|^2 + e^{-(\Omega_{F_3} - \epsilon_e)^2 \frac{\tau_p^2}{4 \ln 2}} \left| C_1 \frac{0.83}{\sqrt{2}} \mathcal{F}(\phi_H(\mathbf{r}))(\mathbf{q}) \right|^2 \right],
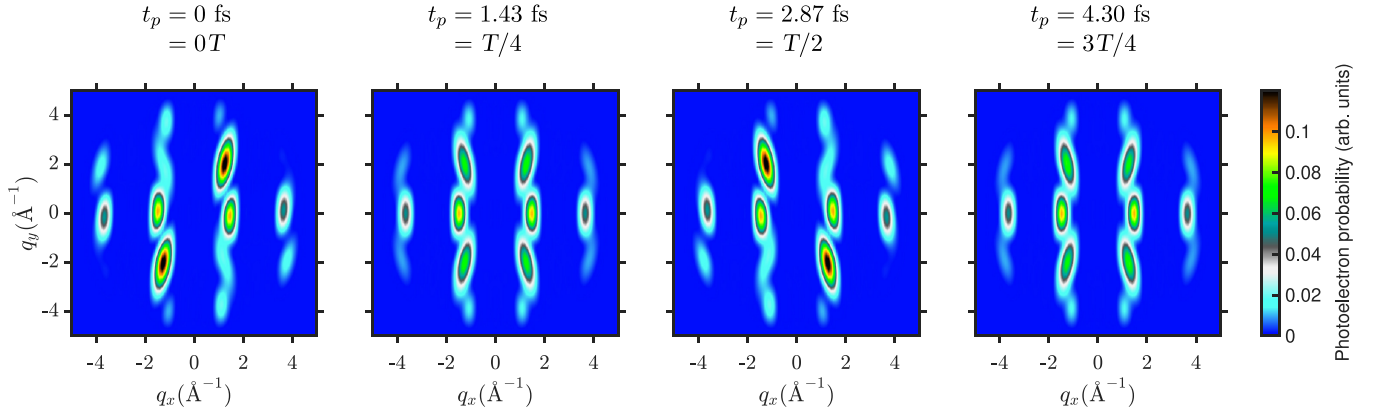\end{aligned} \tag{14}
$$

FIG. 4. Time-dependent photoelectron momentum maps for photoelectrons emitted from the excited pentacene at different probe-pulse arrival times t_p. The probe-pulse duration is 0.5 fs, and the central photon energy is 100 eV. The momentum maps are shown at a photoelectron energy of $\epsilon_e = 99$ eV.

where $\mathcal{F}(\phi(\mathbf{r}))(\mathbf{q}) = (2\pi)^{-3/2} \int dr^3 e^{i\mathbf{q}\cdot\mathbf{r}}\phi(\mathbf{r})$ denotes the Fourier transform of an orbital $\phi(\mathbf{r})$. The resulting time-resolved PMMs shown in Fig. 4 vary strongly with time. The PMMs at $t_p = 0$ and $t_p = \frac{T}{2}$ are the point reflection images of each other and have the same symmetry as the changes in the electron density at these times (see Fig. 2). The PMMs at $t_p = \frac{T}{4}$ and $t_p = \frac{3T}{4}$, when the electron density coincides, are equal and have reflection symmetry. The most pronounced oscillating peaks are located in the PMMs at the momenta $q_x = \pm 1.26$ Å^{-1} and $q_y = \pm 1.97$ Å^{-1}. According to Eq. (14), the time-dependent part of the PMMs arises from the Fourier transform of LUMO and LUMO + 2 orbitals. It is directly related to the negatively charged part of the induced electron-density change (yellow in Fig. 2), which is also specified by the LUMO and LUMO + 2 orbitals [see Eq. (10)]. Thus, the time-dependent features in the PMMs encode the information about the symmetry of the photoinduced electron density. Due to the high contrast of a signal and a low background, these features can be detected in an experiment even if the signal

is weak. Due to the high spatial resolution, PMMs resolve oscillations of the electron density within the molecule.

In Refs. [7,87], we demonstrated that a general time- and momentum-resolved signal from a coherently evolving electronic wave packet can be sensitive to electron currents within a sample. This means that a momentum-resolved signal can be different even when the electron density coincides but the charge flow direction differs. This applies to the electronic state in Fig. 2 at times $t_p = \frac{T}{4}$ and $t_p = \frac{3T}{4}$. However, we do not observe this effect in the considered case since it also averages out due to the high symmetry of the photoinduced charge distribution.

Finally, we investigate PMMs and their temporal dependence at different photoelectron energies in Fig. 5. As follows from the angle-integrated spectra in Fig. 3, the overall intensity of the PMMs increases at lower photoelectron energies. The PMMs at energy $\epsilon_e = 90$ eV and at energy $\epsilon_e = 96$ eV remain almost constant in time, whereas the PMMs at $\epsilon_e = 93$ eV and at $\epsilon_e = 99$ eV show pronounced temporal
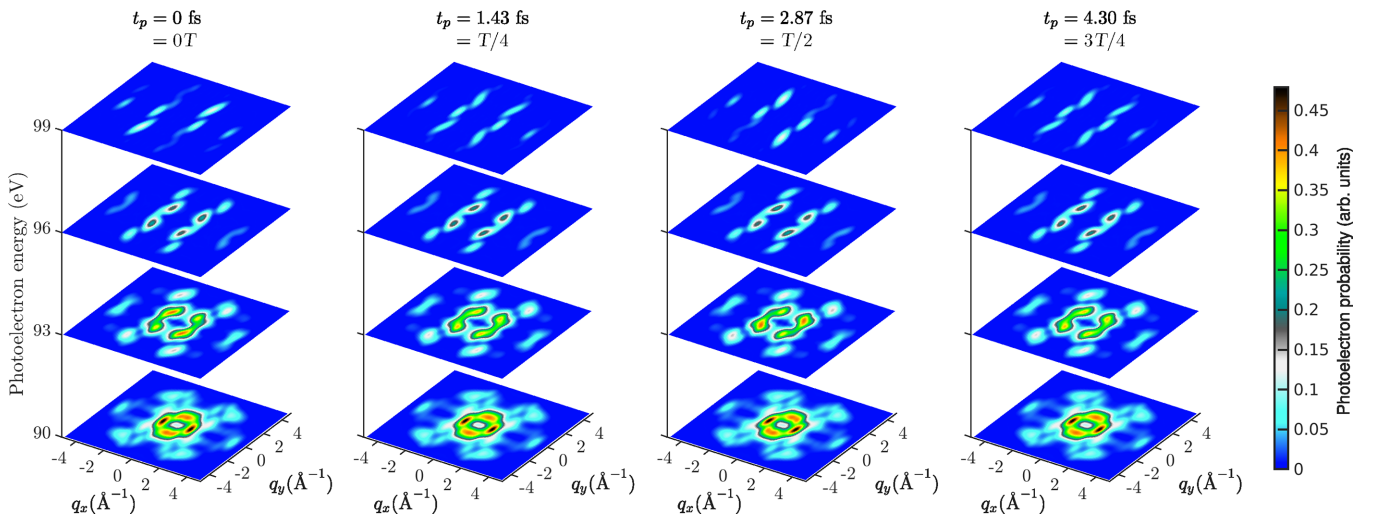

FIG. 5. Time-dependent photoelectron momentum maps for photoelectrons emitted from the excited pentacene for different photoelectron energies ϵ_e. Each set of momentum maps has a different probe-pulse arrival time t_p. The probe-pulse duration is 0.5 fs, and the central photon energy is 100 eV.
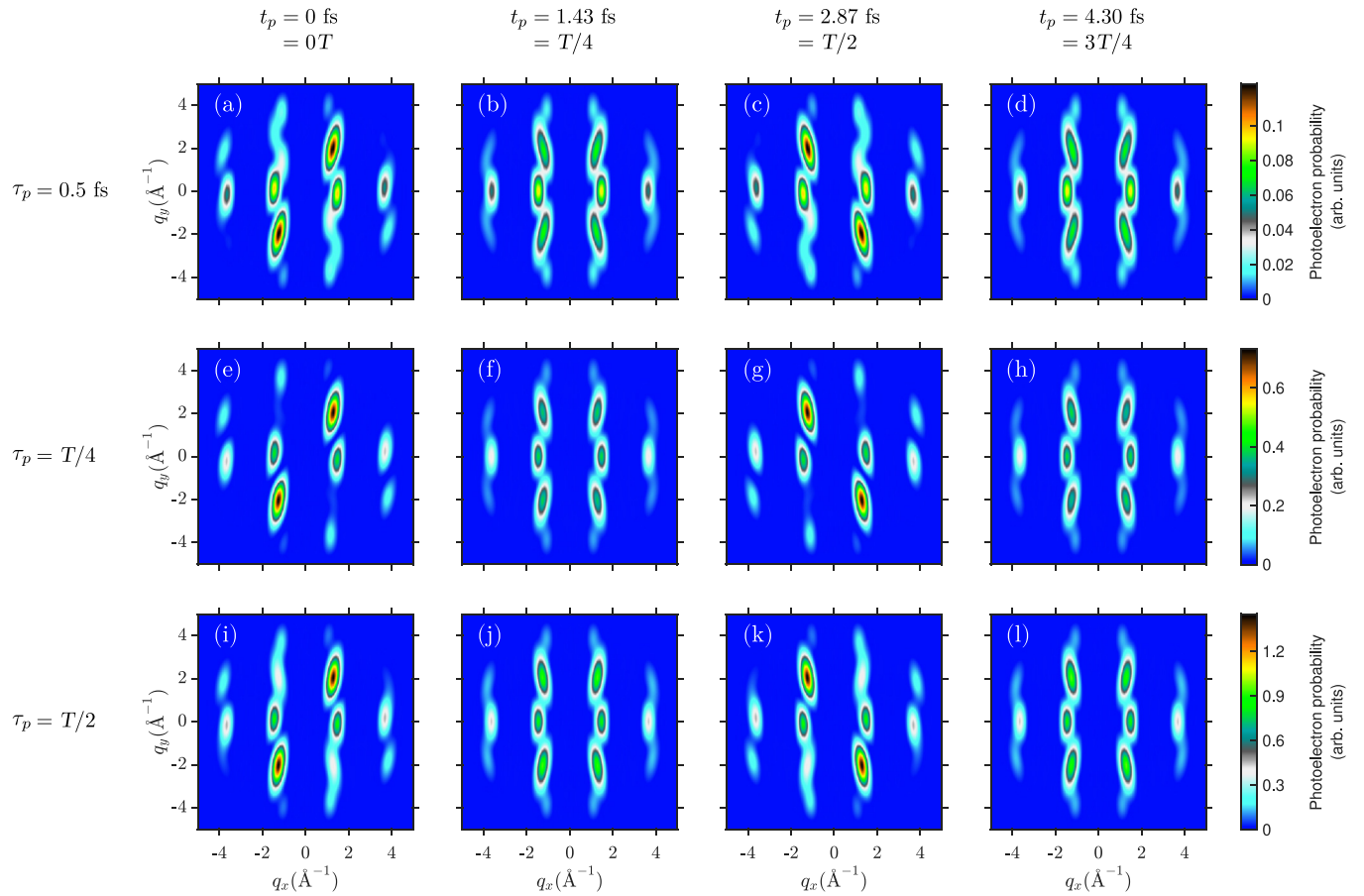
FIG. 6. Time-dependent photoelectron momentum maps (PMMs) for photoelectrons emitted from the excited pentacene. In each column the PMMs are shown for different probe-pulse arrival times: (a), (e), and (i) $t_p = 0T$, (b), (f), and (j) $t_p = T/4$, (c), (g), and (k) $t_p = T/2$, and (d), (h), and (l) $t_p = 3T/4$. In the different rows the PMMs are shown for different probe-pulse durations: (a)–(d) $\tau_p = 0.5$ fs, (e)–(h) $\tau_p = T/4$, and (i)–(l) $\tau_p = T/2$. The probe pulse has a central photon energy of 100 eV. The momentum maps are obtained by averaging the signal over the range of $\epsilon_e = 98.5$ eV to $\epsilon_e = 99.5$ eV to simulate the energy resolution of 1 eV.

dependence. Although the absolute change in the signal in time is approximately the same in the two former cases, the overall contrast is much better for the PMMs at $\epsilon_e = 99$ eV due to a lower time-constant background. This temporal behavior of the signal can be explained by the character of photoinduced changes in the electron density. These changes are due to the electrons photoexcited into orbitals that were unoccupied in the ground state and holes in the orbitals that were doubly occupied in the ground state. If an electron which evolves in the photoexcited orbitals is emitted by a probe pulse, then it directly carries the information about the negatively charged oscillations of the electron density. If an electron is, indeed, emitted from lower-lying orbitals, where an electron hole evolves, then it is an "indirect probe" of the evolving hole. Thus, the signal at the photoelectron energy of 99 eV results from the emission of electrons evolving in the photoexcited orbitals and is the most advantageous to obtain a time-resolved signal with a high contrast.

In a real experiment, PMMs would be obtained with limited energy and time resolution. We simulate the PMMs in the case of limited energy resolution by averaging the photoelectron probability over the corresponding energy interval. We show the PMMs at a photoelectron energy of 99 eV assuming an energy resolution of 1 eV in Figs. 6(a)–6(d), which are

obtained by averaging the signal over the range of 98.5 to 99.5 eV. We find that the momentum distributions are almost unaffected by the limited energy resolution.

The temporal resolution of the experiment is determined by the duration of the probe pulse and the timing jitter between the probe and the pump pulses. If the probe-pulse duration cannot be assumed to be much shorter than the oscillation period, Eq. (3) must be used for the calculation instead of Eq. (2). We calculate the signal with Eq. (3) at different probe-pulse durations τ_p. We also assume a limited energy resolution of 1 eV. As shown in Figs. 6(e)–6(l), the temporal contrast of the resulting signal is quite high even if the probe-pulse duration is as large as a quarter or half of the oscillation period.

In our calculation, we neglected electron-nuclear coupling in the description of charge migration since the primary goal of our study is to investigate how pure electron dynamics on their natural timescale can be measured. Let us discuss which consequences the coupling of electron dynamics to nuclear dynamics would have for the signal. The coupling to nuclear motions would, indeed, lead to decoherence of electron dynamics and should cause the decrease of the oscillation amplitude [41,65,88,89]. Former studies of coupled electron-nuclear dynamics of similar molecules such as norbornadiene

cations [90] and benzene [91] have demonstrated that coherent electron motion can last up to 20 fs in these molecules. It is expected that coherent electronic motion in polycyclic aromatic hydrocarbons, which also include pentacene, would experience similar timescales [91]. Since 20 fs corresponds to about five cycles of oscillation in our case, our assumption that charge migration is coherent during at least one full oscillation period is robust. At longer timescales, the decay of the amplitude of the periodic charge oscillations due to decoherence would result in the decrease of the time-dependent changes in the PMMs. This would lead to a loss of temporal contrast of the signal, which means that the signal at different times would become less distinguishable from the time-independent part of the signal (see Fig. 5). This could even serve as an advantage since such an experiment would reveal the transition of coherent dynamics to decoherent dynamics.

IV. CONCLUSIONS

We showed theoretically how time-resolved photoelectron momentum microscopy can be employed to image photoinduced coherently evolving electron dynamics in a pentacene molecule. The assumed XUV probe pulse of 500-as duration provides the temporal resolution, which is sensitive to pure intramolecular electronic dynamics. The momentum-resolved signal revealed details of electron dynamics with angstrom spatial resolution. Although the angle-averaged photoelectron spectra were not sensitive to electron dynamics, momentum-resolved spectra provided a high-contrast signal evolving in time. At high photoelectron energies, the signal is provided by the electrons emitted from photoexcited orbitals and is not affected by a possible contribution of photoelectrons emitted by molecules that were not photoexcited. Such photoelectron momentum maps are directly related to the negatively charged part of the photoinduced changes in the electron density and is sensitive to its symmetry in real space. These findings demonstrate that attosecond photoelectron momentum microscopy has a big potential to become a novel technique to measure charge migration and electron coherence processes in exciton transport in organic semiconductors with unprecedented time and spatial details.

ACKNOWLEDGMENT

[1] C. Z. Bisgaard, O. J. Clarkin, G. Wu, A. M. D. Lee, O. Geßner, C. C. Hayden, and A. Stolow, Time-resolved molecular frame dynamics of fixed-in-space CS_2 molecules, Science **323**, 1464 (2009).

[2] P. Puschnig, S. Berkebile, A. J. Fleming, G. Koller, K. Emtsev, T. Seyller, J. D. Riley, C. Ambrosch-Draxl, F. P. Netzer, and M. G. Ramsey, Reconstruction of molecular orbital densities from photoemission data, Science **326**, 702 (2009).

[3] D. Lüftner, T. Ules, E. M. Reinisch, G. Koller, S. Soubatch, F. S. Tautz, M. G. Ramsey, and P. Puschnig, Imaging the wave functions of adsorbed molecules, Proc. Natl. Acad. Sci. USA **111**, 605 (2014).

[4] B. Mignolet, R. D. Levine, and F. Remacle, Control of electronic dynamics visualized by angularly resolved photoelectron spectra: A dynamical simulation with an IR pump and XUV attosecond-pulse-train probe, Phys. Rev. A **89**, 021403(R) (2014).

[5] P. Puschnig and D. Lüftner, Simulation of angle-resolved photoemission spectra by approximating the final state by a plane wave: From graphene to polycyclic aromatic hydrocarbon molecules, J. Electron Spectrosc. Relat. Phenom. **200**, 193 (2015).

[6] S. Weiß, D. Lüftner, T. Ules, E. M. Reinisch, H. Kaser, A. Gottwald, M. Richter, S. Soubatch, G. Koller, M. G. Ramsey, F. S. Tautz, and P. Puschnig, Exploring three-dimensional orbital imaging with energy-dependent photoemission tomography, Nat. Commun. **6**, 8287 (2015).

[7] D. Popova-Gorelova, J. Küpper, and R. Santra, Imaging electron dynamics with time- and angle-resolved photoelectron spectroscopy, Phys. Rev. A **94**, 013412 (2016).

[8] P. Kliuiev, T. Latychevskaia, J. Osterwalder, M. Hengsberger, and L. Castiglioni, Application of iterative phase-retrieval algorithms to ARPES orbital tomography, New J. Phys. **18**, 093041 (2016).

[9] C. W. Nicholson, A. Lücke, W. G. Schmidt, M. Puppin, L. Rettig, R. Ernstorfer, and M. Wolf, Beyond the molecular movie: Dynamics of bands and bonds during a photoinduced phase transition, Science **362**, 821 (2018).

[10] P. Kliuiev, G. Zamborlini, M. Jugovac, Y. Gurdal, K. von Arx, K. Waltar, S. Schnidrig, R. Alberto, M. Iannuzzi, V. Feyer, M. Hengsberger, J. Osterwalder, and L. Castiglioni, Combined orbital tomography study of multi-configurational molecular adsorbate systems, Nat. Commun. **10**, 5255 (2019).

[11] C. Metzger, M. Graus, M. Grimm, G. Zamborlini, V. Feyer, M. Schwendt, D. Lüftner, P. Puschnig, A. Schöll, and F. Reinert, Plane-wave final state for photoemission from nonplanar molecules at a metal-organic interface, Phys. Rev. B **101**, 165421 (2020).

[12] G. S. M. Jansen, M. Keunecke, M. Düvel, C. Möller, D. Schmitt, W. Bennecke, F. J. S. Kappert, D. Steil, D. R. Luke, S. Steil, and S. Mathias, Efficient orbital imaging based on ultrafast momentum microscopy and sparsity-driven phase retrieval, New J. Phys. **22**, 063012 (2020).

[13] R. Wallauer, M. Raths, K. Stallberg, L. Münster, D. Brandstetter, X. Yang, J. Güdde, P. Puschnig, S. Soubatch, C. Kumpf, F. C. Bocquet, F. S. Tautz, and U. Höfer, Tracing orbital images on ultrafast time scales, Science **371**, 1056 (2021).

[14] A. Neef, S. Beaulieu, S. Hammer, S. Dong, J. Maklar, T. Pincelli, R. P. Xian, M. Wolf, L. Rettig, J. Pflaum, and R. Ernstorfer, Orbital-resolved observation of singlet fission, arXiv:2204.06824.

[15] K. Baumgärtner, M. Reuner, C. Metzger, D. Kutnyakhov, M. Heber, F. Pressacco, C.-H. Min, T. R. F. Peixoto, M. Reiser, C. Kim, W. Lu, R. Shayduk, M. Izquierdo, G. Brenner, F. Roth,

A. Schöll, S. Molodtsov, W. Wurth, F. Reinert, A. Madsen, D. Popova-Gorelova, and M. Scholz, Ultrafast orbital tomography of a pentacene film using time-resolved momentum microscopy at a FEL, Nat. Commun. **13**, 2741 (2022).

[16] N. Hartmann, G. Hartmann, R. Heider, M. S. Wagner, M. Ilchen, J. Buck, A. O. Lindahl, C. Benko, J. Grünert, J. Krzywinski, J. Liu, A. A. Lutman, A. Marinelli, T. Maxwell, A. A. Miahnahri, S. P. Moeller, M. Planas, J. Robinson, A. K. Kazansky, N. M. Kabachnik *et al.* Attosecond time–energy structure of x-ray free-electron laser pulses, Nat. Photonics **12**, 215 (2018).

[17] P. K. Maroju, C. Grazioli, M. Di Fraia, M. Moioli, D. Ertel, H. Ahmadi, O. Plekan, P. Finetti, E. Allaria, L. Giannessi, G. De Ninno, C. Spezzani, G. Penco, S. Spampinati, A. Demidovich, M. B. Danailov, R. Borghes, G. Kourousias, C. E. S. Dos Reis, F. Billé, A. A. Lutman, R. J. Squibb, Attosecond pulse shaping using a seeded free-electron laser, Nature (London) **578**, 386 (2020).

[18] J. Duris, S. Li, T. Driver, E. G. Champenois, J. P. MacArthur, A. A. Lutman, Z. Zhang, P. Rosenberger, J. W. Aldrich, R. Coffee, G. Coslovich, F.-J. Decker, J. M. Glownia, G. Hartmann, W. Helml, A. Kamalov, J. Knurr, J. Krzywinski, M.-F. Lin, J. P. Marangos, M. Nantel, A. Natan, J. T. O'Neal, N. Shivaram, P. Walter, A. L. Wang, J. J. Welch, T. J. A. Wolf, J. Z. Xu, M. F. Kling, P. H. Bucksbaum, A. Zholents, Z. Huang, J. P. Cryan, and A. Marinelli, Tunable isolated attosecond x-ray pulses with gigawatt peak power from a free-electron laser, Nat. Photonics **14**, 30 (2020).

[19] S. M. Teichmann, F. Silva, S. L. Cousin, M. Hemmer, and J. Biegert, 0.5-keV soft x-ray attosecond continua, Nat. Commun. **7**, 11493 (2016).

[20] J. Li, X. Ren, Y. Yin, K. Zhao, A. Chew, Y. Cheng, E. Cunningham, Y. Wang, S. Hu, Y. Wu, M. Chini, and Z. Chang, 53-attosecond x-ray pulses reach the carbon k-edge, Nat. Commun. **8**, 186 (2017).

[21] X. Ren, J. Li, Y. Yin, K. Zhao, A. Chew, Y. Wang, S. Hu, Y. Cheng, E. Cunningham, Y. Wu, M. Chini, and Z. Chang, Attosecond light sources in the water window, J. Opt. **20**, 023001 (2018).

[22] J. Li, J. Lu, A. Chew, S. Han, J. Li, Y. Wu, H. Wang, S. Ghimire, and Z. Chang, Attosecond science based on high harmonic generation from gases and solids, Nat. Commun. **11**, 2748 (2020).

[23] G. M. Rossi, R. E. Mainz, Y. Yang, F. Scheiba, M. A. Silva-Toledo, S.-H. Chia, P. D. Keathley, S. Fang, O. D. Mücke, C. Manzoni, G. Cerullo, G. Cirmi, and F. X. Kärtner, Sub-cycle millijoule-level parametric waveform synthesizer for attosecond science, Nat. Photonics **14**, 629 (2020).

[24] B. Buades, A. Picón, E. Berger, I. León, N. Di Palo, S. L. Cousin, C. Cocchi, E. Pellegrin, J. H. Martin, S. Mañas-Valero, E. Coronado, T. Danz, C. Draxl, M. Uemoto, K. Yabana, M. Schultze, S. Wall, M. Zürch, and J. Biegert, Attosecond state-resolved carrier motion in quantum materials probed by soft x-ray XANES, Appl. Phys. Rev. **8**, 011408 (2021).

[25] K. Midorikawa, Progress on table-top isolated attosecond light sources, Nat. Photonics **16**, 267 (2022).

[26] F. Calegari, D. Ayuso, A. Trabattoni, L. Belshaw, S. De Camillis, S. Anumula, F. Frassetto, L. Poletto, A. Palacios, P. Decleva, J. B. Greenwood, F. Martín, and M. Nisoli, Ultrafast electron dynamics in phenylalanine initiated by attosecond pulses, Science **346**, 336 (2014).

[27] P. M. Kraus, B. Mignolet, D. Baykusheva, A. Rupenyan, L. Horný, E. F. Penka, G. Grassi, O. I. Tolstikhin, J. Schneider, F. Jensen, L. B. Madsen, A. D. Bandrauk, F. Remacle, and H. J. Wörner, Measurement and laser control of attosecond charge migration in ionized iodoacetylene, Science **350**, 790 (2015).

[28] A. von Conta, A. Tehlar, A. Schletter, Y. Arasaki, K. Takatsuka, and H. J. Wörner, Conical-intersection dynamics and ground-state chemistry probed by extreme-ultraviolet time-resolved photoelectron spectroscopy, Nat. Commun. **9**, 3162 (2018).

[29] F. Langer, C. P. Schmid, S. Schlauderer, M. Gmitra, J. Fabian, P. Nagler, C. Schüller, T. Korn, P. G. Hawkins, J. T. Steiner, U. Huttner, S. W. Koch, M. Kira, and R. Huber, Lightwave valleytronics in a monolayer of tungsten diselenide, Nature (London) **557**, 76 (2018).

[30] F. Siegrist, J. A. Gessner, M. Ossiander, C. Denker, Y.-P. Chang, M. C. Schröder, A. Guggenmos, Y. Cui, J. Walowski, U. Martens, J. K. Dewhurst, U. Kleineberg, M. Münzenberg, S. Sharma, and M. Schultze, Light-wave dynamic control of magnetism, Nature (London) **571**, 240 (2019).

[31] P. Peng, C. Marceau, and D. M. Villeneuve, Attosecond imaging of molecules using high harmonic spectroscopy, Nat. Rev. Phys. **1**, 144 (2019).

[32] J. P. Marangos, Accessing the quantum spatial and temporal scales with XFELS, Nat. Rev. Phys. **2**, 332 (2020).

[33] K. S. Zinchenko, F. Ardana-Lamas, I. Seidu, S. P. Neville, J. van der Veen, V. U. Lanfaloni, M. S. Schuurman, and H. J. Wörner, Sub-7-femtosecond conical-intersection dynamics probed at the carbon k-edge, Science **371**, 489 (2021).

[34] M. Rebholz *et al.*, All-XUV Pump-Probe Transient Absorption Spectroscopy of the Structural Molecular Dynamics of Di-iodomethane, Phys. Rev. X **11**, 031001 (2021).

[35] D. Garratt, L. Misiekis, D. Wood, E. W. Larsen, M. Matthews, O. Alexander, P. Ye, S. Jarosch, C. Ferchaud, C. Strüber, A. S. Johnson, A. A. Bakulin, T. J. Penfold, and J. P. Marangos, Direct observation of ultrafast exciton localization in an organic semiconductor with soft x-ray transient absorption spectroscopy, Nat. Commun. **13**, 3414 (2022).

[36] E. P. Månsson, S. Latini, F. Covito, V. Wanie, M. Galli, E. Perfetto, G. Stefanucci, U. De Giovannini, M. C. Castrovilli, A. Trabattoni, F. Frassetto, L. Poletto, J. B. Greenwood, F. Légaré, M. Nisoli, A. Rubio, and F. Calegari, Ultrafast dynamics of adenine following XUV ionization, J. Phys.: Photonics **4**, 034003 (2022).

[37] G. Dixit, O. Vendrell, and R. Santra, Imaging electronic quantum motion with light, Proc. Natl. Acad. Sci. USA **109**, 11636 (2012).

[38] D. Popova-Gorelova and R. Santra, Imaging instantaneous electron flow with ultrafast resonant x-ray scattering, Phys. Rev. B **91**, 184303 (2015).

[39] D. Popova-Gorelova and R. Santra, Imaging interatomic electron current in crystals with ultrafast resonant x-ray scattering, Phys. Rev. B **92**, 184304 (2015).

[40] M. Hollstein, R. Santra, and D. Pfannkuche, Correlation-driven charge migration following double ionization and attosecond transient absorption spectroscopy, Phys. Rev. A **95**, 053411 (2017).

[41] V. Despré, N. V. Golubev, and A. I. Kuleff, Charge Migration in Propiolic Acid: A Full Quantum Dynamical Study, Phys. Rev. Lett. **121**, 203002 (2018).

[42] M. He, Y. Li, Y. Zhou, M. Li, W. Cao, and P. Lu, Direct Visualization of Valence Electron Motion Using Strong-Field Photoelectron Holography, Phys. Rev. Lett. **120**, 133204 (2018).

[43] K.-J. Yuan and A. D. Bandrauk, Ultrafast x-ray photoelectron imaging of attosecond electron dynamics in molecular coherent excitation, J. Phys. Chem. A **123**, 1328 (2019).

[44] L. Inhester, L. Greenman, A. Rudenko, D. Rolles, and R. Santra, Detecting coherent core-hole wave-packet dynamics in N_2 by time- and angle-resolved inner-shell photoelectron spectroscopy, J. Chem. Phys. **151**, 054107 (2019).

[45] K. Khalili, L. Inhester, C. Arnold, A. S. Gertsen, J. W. Andreasen, and R. Santra, Simulation of time-resolved x-ray absorption spectroscopy of ultrafast dynamics in particle-hole-excited 4-(2-thienyl)-2, 1, 3-benzothiadiazole, Struct. Dyn. **7**, 044101 (2020).

[46] S. M. Cavaletto, D. Keefer, J. R. Rouxel, F. Aleotti, F. Segatta, M. Garavelli, and S. Mukamel, Unveiling the spatial distribution of molecular coherences at conical intersections by covariance x-ray diffraction signals, Proc. Natl. Acad. Sci. USA **118**, e2105046118 (2021).

[47] F. Mauger, A. S. Folorunso, K. A. Hamer, C. Chandre, M. B. Gaarde, K. Lopata, and K. J. Schafer, Charge migration and attosecond solitons in conjugated organic molecules, Phys. Rev. Res. **4**, 013073 (2022).

[48] Y. Nam, F. Montorsi, D. Keefer, S. M. Cavaletto, J. Y. Lee, A. Nenov, M. Garavelli, and S. Mukamel, Time-resolved optical pump-resonant x-ray probe spectroscopy of 4-thiouracil: A simulation study, J. Chem. Theory Comput. **18**, 3075 (2022).

[49] K. Chordiya, V. Despré, B. Nagyillés, F. Zeller, Z. Diveki, A. I. Kuleff, and M. U. Kahaly, Photo-ionization initiated differential ultrafast charge migration: Impact of molecular symmetries and tautomeric forms, Phys. Chem. Chem. Phys. (2023), doi: 10.1039/D2CP02681C.

[50] S. Yoo, B. Domercq, and B. Kippelen, Efficient thin-film organic solar cells based on pentacene/C_{60} heterojunctions, Appl. Phys. Lett. **85**, 5427 (2004).

[51] K. Leo, Organic photovoltaics, Nat. Rev. Mater. **1**, 16056 (2016).

[52] A. Köhler and H. Bässler, *Electronic Processes in Organic Semiconductors: An Introduction* (Wiley, Hoboken, NJ, 2015).

[53] F. Fassioli, R. Dinshaw, P. C. Arpin, and G. D. Scholes, Photosynthetic light harvesting: Excitons and coherence, J. R. Soc. Interface **11**, 20130901 (2014).

[54] T. R. Nelson, D. Ondarse-Alvarez, N. Oldani, B. Rodriguez-Hernandez, L. Alfonso-Hernandez, J. F. Galindo, V. D. Kleiman, S. Fernandez-Alberti, A. E. Roitberg, and S. Tretiak, Coherent exciton-vibrational dynamics and energy transfer in conjugated organics, Nat. Commun. **9**, 2316 (2018).

[55] S. Rafiq and G. D. Scholes, From fundamental theories to quantum coherences in electron transfer, J. Am. Chem. Soc. **141**, 708 (2019).

[56] L. S. Cederbaum and J. Zobeley, Ultrafast charge migration by electron correlation, Chem. Phys. Lett. **307**, 205 (1999).

[57] J. Breidbach and L. S. Cederbaum, Migration of holes: Formalism, mechanisms, and illustrative applications, J. Chem. Phys. **118**, 3983 (2003).

[58] A. I. Kuleff, S. Lünnemann, and L. S. Cederbaum, Ultrafast charge migration following ionization in oligopeptides, in *Ul-*

trafast Phenomena XVI, edited by P. Corkum, S. Silvestri, K. A. Nelson, E. Riedle, and R. W. Schoenlein (Springer, Berlin, 2009), pp. 586–588.

[59] S. Lünnemann, A. I. Kuleff, and L. S. Cederbaum, Charge migration following ionization in systems with chromophore-donor and amine-acceptor sites, J. Chem. Phys. **129**, 104305 (2008).

[60] A. D. Dutoi, L. S. Cederbaum, M. Wormit, J. H. Starcke, and A. Dreuw, Tracing molecular electronic excitation dynamics in real time and space, J. Chem. Phys. **132**, 144302 (2010).

[61] A. D. Dutoi, M. Wormit, and L. S. Cederbaum, Ultrafast charge separation driven by differential particle and hole mobilities, J. Chem. Phys. **134**, 024303 (2011).

[62] A. D. Dutoi and L. S. Cederbaum, An excited electron avoiding a positive charge, J. Phys. Chem. Lett. **2**, 2300 (2011).

[63] F. Remacle and R. D. Levine, Attosecond pumping of nonstationary electronic states of LiH: Charge shake-up and electron density distortion, Phys. Rev. A **83**, 013411 (2011).

[64] A. I. Kuleff and L. S. Cederbaum, Ultrafast correlation-driven electron dynamics, J. Phys. B **47**, 124002 (2014).

[65] H. J. Wörner, C. A. Arrell, N. Banerji, A. Cannizzo, M. Chergui, A. K. Das, P. Hamm, U. Keller, P. M. Kraus, E. Liberatore, P. Lopez-Tarifa, M. Lucchini, M. Meuwly, C. Milne, J.-E. Moser, U. Rothlisberger, G. Smolentsev, J. Teuscher, J. A. van Bokhoven, and O. Wenger, Charge migration and charge transfer in molecular systems, Struct. Dyn. **4**, 061508 (2017).

[66] T. Kuś, B. Mignolet, R. D. Levine, and F. Remacle, Pump and probe of ultrafast charge reorganization in small peptides: A computational study through sudden ionizations, J. Phys. Chem. A **117**, 10513 (2013).

[67] A. Stolow, A. E. Bragg, and D. M. Neumark, Femtosecond time-resolved photoelectron spectroscopy, Chem. Rev. **104**, 1719 (2004).

[68] K.-J. Yuan, C.-C. Shu, D. Dong, and A. D. Bandrauk, Attosecond dynamics of molecular electronic ring currents, J. Phys. Chem. Lett. **8**, 2229 (2017).

[69] A. Marciniak, V. Despré, V. Loriot, G. Karras, M. Hervé, L. Quintard, F. Catoire, C. Joblin, E. Constant, A. I. Kuleff, and F. Lépine, Electron correlation driven non-adiabatic relaxation in molecules excited by an ultrashort extreme ultraviolet pulse, Nat. Commun. **10**, 337 (2019).

[70] D. Jadoun and M. Kowalewski, Time-resolved photoelectron spectroscopy of conical intersections with attosecond pulse trains, J. Phys. Chem. Lett. **12**, 8103 (2021).

[71] D. Dowek and P. Decleva, Trends in angle-resolved molecular photoelectron spectroscopy, Phys. Chem. Chem. Phys. **24**, 24614 (2022).

[72] S. Hüfner, *Very High Resolution Photoelectron Spectroscopy*, Lecture Notes in Physics, Vol. 715 (Springer, 2007).

[73] B. Mignolet, R. D. Levine, and F. Remacle, Localized electron dynamics in attosecond-pulse-excited molecular systems: Probing the time-dependent electron density by sudden photoionization, Phys. Rev. A **86**, 053429 (2012).

[74] A. Perveaux, D. Lauvergnat, F. Gatti, G. J. Halász, Á. Vibók, and B. Lasorne, Monitoring the birth of an electronic wavepacket in a molecule with attosecond time-resolved photoelectron spectroscopy, J. Phys. Chem. A **118**, 8773 (2014).

[75] B. Mignolet, R. D. Levine, and F. Remacle, Charge migration in the bifunctional PENNA cation induced and probed by ultrafast ionization: A dynamical study, J. Phys. B **47**, 124011 (2014).

[76] P. Puschnig, E.-M. Reinisch, T. Ules, G. Koller, S. Soubatch, M. Ostler, L. Romaner, F. S. Tautz, C. Ambrosch-Draxl, and M. G. Ramsey, Orbital tomography: Deconvoluting photoemission spectra of organic molecules, Phys. Rev. B **84**, 235427 (2011).

[77] B. Stadtmüller, M. Willenbockel, E. M. Reinisch, T. Ules, F. C. Bocquet, S. Soubatch, P. Puschnig, G. Koller, M. G. Ramsey, F. S. Tautz, and C. Kumpf, Orbital tomography for highly symmetric adsorbate systems, Europhys. Lett. **100**, 26008 (2012).

[78] P. A. Malmqvist, A. Rendell, and B. O. Roos, The restricted active space self-consistent-field method, implemented with a split graph unitary group approach, J. Phys. Chem. **94**, 5477 (1990).

[79] F. Aquilante *et al.*, Molcas 8: New capabilities for multiconfigurational quantum chemical calculations across the periodic table, J. Comput. Chem. **37**, 506 (2016).

[80] T. H. Dunning, Gaussian basis sets for use in correlated molecular calculations. I. The atoms boron through neon and hydrogen, J. Chem. Phys. **90**, 1007 (1989).

[81] B. P. Pritchard, D. Altarawy, B. Didier, T. D. Gibson, and T. L. Windus, New basis set exchange: An open, up-to-date resource for the molecular sciences community, J. Chem. Inf. Model. **59**, 4814 (2019).

[82] G. Kovačević and V. Veryazov, Luscus: Molecular viewer and editor for molcas, J. Cheminf. **7**, 16 (2015).

[83] E. Heinecke, D. Hartmann, R. Müller, and A. Hese, Laser spectroscopy of free pentacene molecules (i): The rotational structure of the vibrationless s1 ← s0 transition, J. Chem. Phys. **109**, 906 (1998).

[84] S. Grimme and M. Parac, Substantial errors from time-dependent density functional theory for the calculation of excited states of large π systems, Chem. Phys. Chem. **4**, 292 (2003).

[85] P. B. Coto, S. Sharifzadeh, J. B. Neaton, and M. Thoss, Low-lying electronic excited states of pentacene oligomers: A comparative electronic structure study in the context of singlet fission, J. Chem. Theory Comput. **11**, 147 (2015).

[86] K. Momma and F. Izumi, *VESTA3* for three-dimensional visualization of crystal, volumetric and morphology data, J. Appl. Crystallogr. **44**, 1272 (2011).

[87] D. Popova-Gorelova, Imaging electron dynamics with ultrashort light pulses: A theory perspective, Appl. Sci. **8**, 318 (2018).

[88] C. Arnold, O. Vendrell, and R. Santra, Electronic decoherence following photoionization: Full quantum-dynamical treatment of the influence of nuclear motion, Phys. Rev. A **95**, 033425 (2017).

[89] D. T. Matselyukh, V. Despré, N. V. Golubev, A. I. Kuleff, and H. J. Wörner, Decoherence and revival in attosecond charge migration driven by non-adiabatic dynamics, Nat. Phys. **18**, 1206 (2022).

[90] A. J. Jenkins, M. Vacher, R. M. Twidale, M. J. Bearpark, and M. A. Robb, Charge migration in polycyclic norbornadiene cations: Winning the race against decoherence, J. Chem. Phys. **145**, 164103 (2016).

[91] V. Despré, A. Marciniak, V. Loriot, M. C. E. Galbraith, A. Rouzée, M. J. J. Vrakking, F. Lépine, and A. I. Kuleff, Attosecond hole migration in benzene molecules surviving nuclear motion, J. Phys. Chem. Lett. **6**, 426 (2015).